Draft version August 26, 2016
Preprint typeset using LaTeX style emulateapj v. 12/16/11

COSMOLOGICAL CONSTRAINTS FROM THE REDSHIFT DEPENDENCE OF THE GALAXY ANGULAR 2-POINT CORRELATION FUNCTION

Xiao-Dong Li,
School of Physics, Korea Institute for Advanced Study, 85 Heogiro, Dongdaemun-gu, Seoul 130-722, Korea

Cheng Cheng,
Kavli Institute for Theoretical Physics China, Institute of Theoretical Physics, Chinese Academy of Sciences, Zhong Guan Cun Street 55#, Beijing, 100190, P.R. China and
University of Chinese Academy of Sciences, P.R. China

Changbom Park,
School of Physics, Korea Institute for Advanced Study, 85 Heogiro, Dongdaemun-gu, Seoul 130-722, Korea

Cristiano G. Sabiu, Hyunbae Park,
Korea Astronomy and Space Science Institute, Daejeon 305-348, Korea

Juhan Kim[1],
Center for Advanced Computation, Korea Institute for Advanced Study, 85 Hoegi-ro, Dongdaemun-gu, Seoul 130-722, Korea and
School of Physics, Korea Institute for Advanced Study, 85 Heogiro, Dongdaemun-gu, Seoul 130-722, Korea

and

Sungwook E. Hong
School of Physics, Korea Institute for Advanced Study, 85 Heogiro, Dongdaemun-gu, Seoul 130-722, Korea
Draft version August 26, 2016

ABSTRACT

We use the shape of galaxy 2-point correlation function to measure the redshift dependence cosmology volume effect. ...
Keywords: large-scale structure of Universe — dark energy — cosmological parameters

1. INTRODUCTION

Dark energy ... Large scale structure...

2pCF is a good statistic... blahblah In 2d xi(s,mu) ... In *** we used the redshift dependence of 2pCF to probe the volume and AP effect... The method is applied to BOSS data in *** and obtain tight constraint...

In *** we further propose to use the shape of xi(s) to probe the volume effect... Stretch or compression shifts the clustering properties in some particular scale to larger or smaller scales... The shape of measured xi(s) is thus stretched or compressed.

The outline of this paper is as follows.

This paper is organized as follows... The outline of this paper proceeds as follows. In §2 we briefly review the nature and consequences of the AP effect and volume changes when performing coordinate transforms in a cosmological context. In §3 we describe the N-body simulations and mock galaxy catalogues that are used to test our methodology. In §4, we describe our new analysis method for quantifying the redshift dependence of volume effect. We conclude in §5.

2. GEOMETRIC DEFORMATION WHEN

In this section we briefly introduce the scaling effect in wrongly assumed cosmologies. A more detailed description has been provided in Li et al. (2014, 2015, 2016).

Suppose that we are probing the shape of some objects in the Universe. We measure its redshift span Δz and angular size $\Delta\theta$, then compute its sizes in the radial and transverse directions from the relations of

$$\Delta r_{\parallel} = \frac{c}{H(z)}\Delta z, \quad \Delta r_{\perp} = (1+z)D_A(z)\Delta\theta, \qquad (1)$$

where H is the Hubble parameter, D_A is the angular diameter distance. In the particular case of a flat universe with constant dark energy EoS, they take the forms of

$$H(z) = H_0\sqrt{\Omega_m a^{-3} + (1-\Omega_m)a^{-3(1+w)}},$$
$$D_A(z) = \frac{1}{1+z}r(z) = \frac{1}{1+z}\int_0^z \frac{dz'}{H(z')}, \qquad (2)$$

where $a = 1/(1+z)$ is the cosmic scale factor, H_0 is the present value of Hubble parameter and $r(z)$ is the comoving distance.

In case we adopted a wrong set of cosmological parameters in Equation (1,2), the inferred $\Delta r_{\parallel}$ and $\Delta r_{\perp}$ are wrong, resulting in distorted shape (AP effect) and wrongly estimated volume (volume effect). These effects have been discussed in Li et al. (2014, 2015, 2016). This paper we focus on the misestimation of $\Delta r_{\perp}$,which can be described by the following quantities

$$\frac{\Delta r_{\perp,\rm wrong}}{\Delta r_{\perp,\rm true}} = \frac{D_{A,\rm wrong}}{D_{A,\rm true}}, \qquad (3)$$

where “true” and “wrong” denote the values of D_A in the true cosmology and wrongly assumed cosmology.

[1] Corresponding Author: kjhan@kias.re.kr

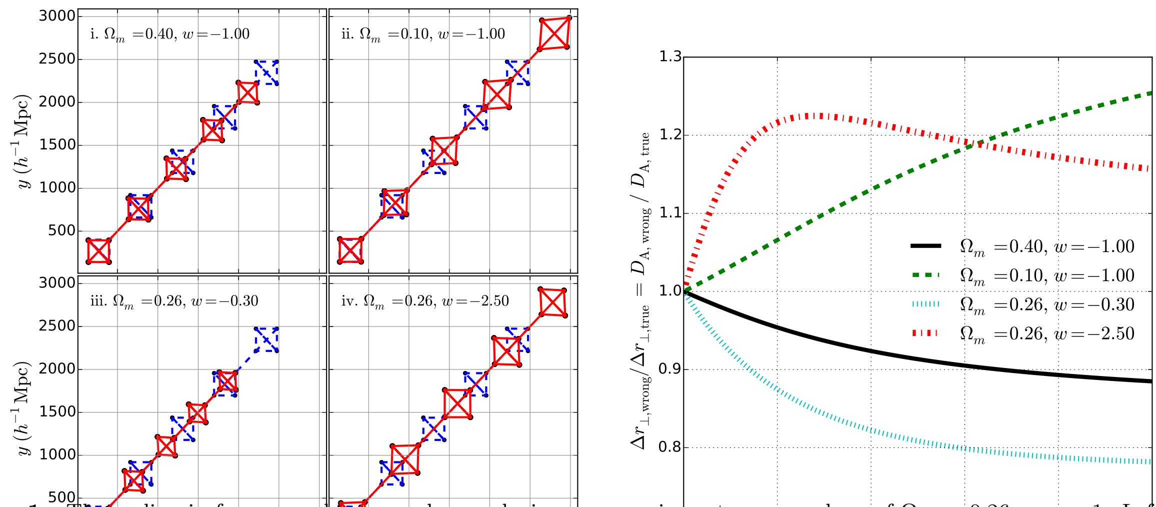

Figure 1. The scaling in four wrongly assumed cosmologies ..., assuming a true cosmology of $\Omega_m = 0.26$, $w = -1$. Left panel shows a series of circular objects, measured by an observer located at the origin. Their true positions and shapes are plotted in blue dashed lines. The observer measures the redshifts of these objects, adopts the wrong cosmologies to compute the distance, and obtains wrong results (the red solid lines). Right panel shows the misestimation of angular diameter distance when the wrong cosmologies are adopted.

The effects due to wrongly assumed cosmological parameters are shown in the upper panel of Figure 1. Suppose that the true cosmology is a flat ΛCDM with present density parameter $\Omega_m = 0.26$ and standard dark energy EoS $w = -1$. If we were to distribute a series of perfect squares at various distances from 500 Mpc/h to ???? Mpc/h, and an observer located at the origin were to measure their redshifts and compute their positions and shapes using redshift-distance relations of ??? incorrect cosmologies (TBM)

1. $\Omega_m = 0.41$, $w = -1.3$,

2. $\Omega_m = 0.11$, $w = -0.7$,

the shapes of the squares appear distorted (AP effect), and their volumes are changed (volume effect). In the cosmological model (ii) with $\Omega_m = 0.11$, $w = -0.7$, we see a stretch of the shape in the line of sight (LOS) direction (hereafter "LOS shape stretch") and magnification of the volume (hereafter "volume magnification"), while in the model with $\Omega_m = 0.41$, $w = -1.3$, we see opposite effects of LOS shape compression and volume shrinkage.

In the lower panel of Figure 1, we plot the $\frac{\Delta r_{\perp,\mathrm{wrong}}}{\Delta r_{\perp,\mathrm{true}}}$ redshift. In cosmology (i), both quantities have values less than 1, indicating LOS shape compression and volume shrink. The effect in cosmology (ii) is slightly more subtle. At low redshift, the effect of dark energy is important, and there is LOS shape compression and volume reduction due to the quintessence like dark energy EoS. However, at higher redshift the role of dark matter is more important, and we see LOS shape stretch and volume magnification due to the small Ω_m.

More importantly, Figure 1 highlights the redshift dependence of the AP and volume effects. For example, in the cosmology with $\Omega_m = 0.41$, $w = -1.3$, both the LOS shape stretch and volume magnification become more significant with increasing redshift. In the cosmology with $\Omega_m = 0.11$, $w = -0.7$, not only do the magnitudes of the effects evolve with redshift, but there is also a turnover from LOS shape compression and volume shrink at lower redshift to LOS shape stretch and volume magnification at higher redshift.s

3. THE SIMULATION DATA

We test the method on the Horizon Run 4 (HR4) simulation (Kim et al. 2015). HR4 used $N = 6300^3$ particles in a box size of $L = 3150\ h^{-1}$Mpc. It adopted the second order Lagrangian perturbation theory (2LPT) initial conditions at $z_i = 100$ and a WMAP5 cosmology $(\Omega_b, \Omega_m, \Omega_\Lambda, h, \sigma_8, n_s) = (0.044,\ 0.26,\ 0.74,\ 0.72,\ 0.79,\ 0.96)$ (Komatsu et al. 2011). The particle mass is $\simeq m_p \simeq 9.02 \times 10^9 h^{-1}\mathrm{M}_\odot$.

Mock galaxy samples are produced from the simulation based on a modified one-to-one correspondence scheme (Hong et al. 2016). The most bound member particles (MBPs) of simulated halos are adopted as the tracer of galaxies, and the merger timescale is computed to get the lifetime of merged halos. Merger trees of simulated halos are constructed by tracking their MBPs from $z = 12$ to 0. When a merger event occurs, we adopt the formular of Jiang et al. (2008) to calculate the merger timescale and determine when a satellite galaxy is completely disrupted.

Hong et al. (2016) compared the 2pCF of the SDSS DR7 volume-limited galaxy sample (Zehavi et al. 2011) and the HR4 $z = 0$ mock galaxies. The mock galaxies shows a similar finger of god (FOG) feature (Jackson 1972) as the observation. On scales greater than 1 h^{-1}Mpc., the projected 2pCF of the mock and observational samples agree within 1σ deviation.

The output of HR4 simulation includes one all-sky light cone mock galaxy catalogue reaching $r = 3\,150\ h^{-1}$Mpc and a series (**how many?**) of snapshot mock galaxy catalogues at different redshifts. In this paper we use five snapshot data at $z = 0, 0.5, 1, 1.5, 2$. We require subhalos to have at least 30 member particles, so the minimal mass of galaxies is $\simeq m_p \simeq 2.7 \times 10^{11} h^{-1}\mathrm{M}_\odot$. At the five redshifts, we get a number of 457, 406, 352, 206 and 228 million mock galaxies, corresponding to a number density of 1.46, 1.30, 1.13, 0.98 and 0.73 in unit of $10^{-2}h^3\mathrm{Mpc}^{-3}$, respectively.

4. METHODOLOGY

We measure the angular 2pCF in the five redshifts. We determine cosmological parameters by examining the redshift evolution of clustering anisotropy. Mock survey samples are used to correct the results for the systematics and to estimate the covariance.

4.1. *Grid of cosmology parameters*

The observed coordinates (*RA, Dec, z*) of galaxies need to be converted to comoving coordinates (*x, y, z*) for the 2pCF analysis. The dependence of clustering anisotropy on cosmology enters through the conversion from redshift to comoving distance, i.e. the distance-redshift relation $r(z)$. We consider the case of a flat Universe dominated by matter and dark energy, so our $r(z)$ is governed by two parameters, Ω_m and w, as presented in Equation (2) .

To constrain these two parameters we examine the parameter space of $0.06 \leq \Omega_m \leq 0.41$ and $-1.5 \leq w \leq -0.4$ with intervals of $\delta\Omega_m = 0.005$ and $\delta w = 0.025$, forming a 71×45 grid. For each set of (Ω_m, w), the comoving coordinates of all galaxies are computed, and the 2pCF is ready to be calculated.

4.2. *Measuring the correlation function*

We adopt the Landy-Szalay estimator (Landy & Szalay 1993) to calculate the 2pCF,

$$\xi(s,\mu) = \frac{DD - 2DR + RR}{RR} \ , \tag{4}$$

where DD is the number of galaxy–galaxy pairs, DR the number of galaxy-random pairs, and RR is the number of random–random pairs, all separated by a distance defined by $s \pm \Delta s$ and $\mu \pm \Delta\mu$, where s is the distance between the pair and $\mu = \cos(\theta)$, with θ being the angle between the line joining the pair of galaxies and the LOS direction to the target galaxy. This statistic captures the anisotropy of the clustering signal.

The random catalogue consists of unclustered points whose number density in redshift space mimics the radial selection function of the observational data. To reduce the statistical variance of the estimator we use 50 times as many random points as we have galaxies. The galaxies and random points are weighted as described in Sec. 3.

Figure 4 shows the 2D contour of measured ξ as a function of μ and s, from the six redshift bins of LOWZ and CMASS samples in the cosmology of $\Omega_m = 0.31$ ΛCDM model. Due to the peculiar velocity effect, the contour lines are not horizontal. The FOG (Jackson 1972) and Kaiser (Kaiser 1987) effects clearly manifest themselves through the tilting of contour lines in regions of $\mu \to 1$ and $1-\mu \gtrsim 0.1$, respectively. A visual inspection of the contour maps from the six redshift bins reveals that they all have a similar appearance, implying small redshift evolution of ξ.

4.3. *Probing the anisotropy through 2pCF*

The 2pCF is measured as a function of the separation s and the angular direction μ. To probe the anisotropy we are more interested in the dependence of the 2pCF on μ. We follow the procedure of Li et al. (2015) and integrate the ξ over the interval $s_{\max} \leq s \leq s_{\min}$. We evaluate

$$\xi_{\Delta s}(\mu) \equiv \int_{s_{\min}}^{s_{\max}} \xi(s,\mu)\ ds. \tag{5}$$

The integration is limited at both small and large scales. At small scales the value of ξ is seriously affected by the FOG effect (Jackson 1972) which depends on the galaxies bias. This may introduce a redshift evolution in $\xi_{\Delta s}(\mu)$ that is relatively difficult to model. At large scales the measurement is dominated by noise due to poor statistics. Li et al. (2015) found that $s_{\min} = 6 - 10$ h^{-1}Mpc and $s_{\max} = 40 - 70$ h^{-1}Mpc are reasonable choices which provide consistent, tight and unbiased constraints on cosmological parameters. In this analysis we choose $s_{\min} = 6\ h^{-1}$Mpc and $s_{\max} = 40\ h^{-1}$Mpc.

The redshift evolution of the bias of observed galaxies leads to redshift evolution of the strength of clustering, which is difficult to accurately model. To mitigate this systematic uncertainty we rely on the shape of $\xi_{\Delta s}(\mu)$, rather than its amplitude,

$$\hat{\xi}_{\Delta s}(\mu) \equiv \frac{\xi_{\Delta s}(\mu)}{\int_0^{\mu_{\max}} \xi_{\Delta s}(\mu)\ d\mu}. \tag{6}$$

We impose a cut $\mu < \mu_{\max}$ to reduce the fiber collision and FOG effects which are stronger toward the LOS ($\mu \to 1$) direction.

The clustering properties may be affected by various properties of the galaxy sample, such as, for example the mass, morphology, color, concentration. In our simulation, using the merger tree, we identify "galaxies", therefore we only use the galaxy mass building history to simulate BOSS galaxies. Therefore, it is necessary for us to test if our mock galaxies can accurately reproduce the $\hat{\xi}_{\Delta s}(\mu)$ of observed galaxies.

Figure **??** compares the shape of $\hat{\xi}_{\Delta s}(\mu)$ measured from observational data and mock survey samples. It is clear that $\hat{\xi}_{\Delta s}(\mu)$ from mock galaxies identified in the HR4 simulation (green dotted line) agrees well with the observation. The enhancement near $\theta = 0°$ is caused by the FOG effect, and the characteristic shape in $20° \lesssim \theta \lesssim 90°$ produced from the large-scale flow are all very well reproduced. This result verifies the ability of our mock galaxies to reproduce the clustering properties of the observed galaxies. The small overestimate (underestimate) of $\hat{\xi}_{\Delta s}$ at large (small) μ could be due to that our mocks galaxies are more massive than those in the observations. We use the HR4 galaxy mocks to correct the systematics.

We divide the full angular range $0 \leq \mu \leq \mu_{\max}$ into n_μ bins and measure its value in each bin. Since we are free to choose $\mu_{\max}$ and n_μ, they are varied to optimize the S/N of our results. This topic will be discussed in Sec. **??**.

4.4. *Characterizing the redshift evolution*

As shown in Figure **??**, we split the BOSS DR12 galaxies into six redshift bins, three in LOWZ and three in CMASS. To study the redshift evolution of the clustering anisotropy we use the *first redshift bin* as the reference and compare the measurements in other bins with that in the first. We define

$$\delta\hat{\xi}_{\Delta s}(z_i, z_1, \mu_j)\ \equiv\ \hat{\xi}_{\Delta s}(z_i,\mu_j) - \hat{\xi}_{\Delta s}(z_1,\mu_j) \tag{7}$$

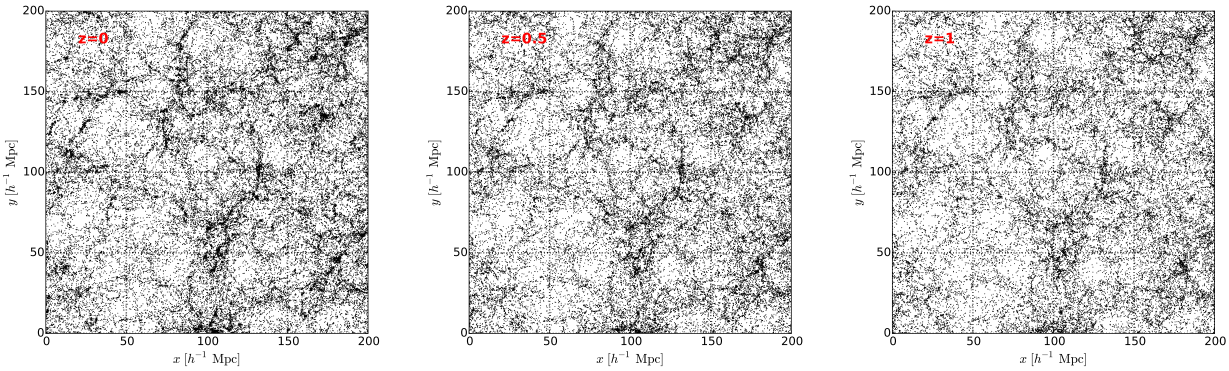

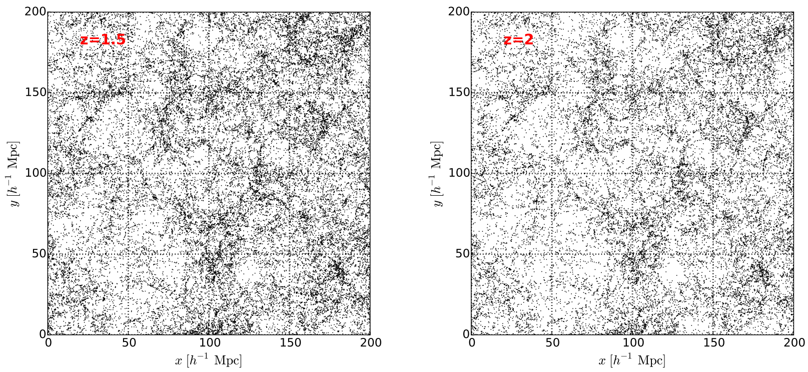

Figure 2. blah

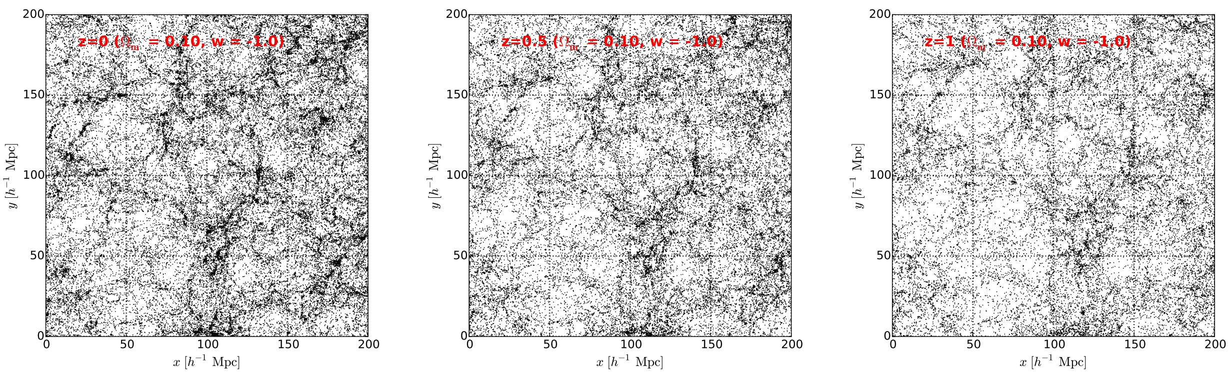

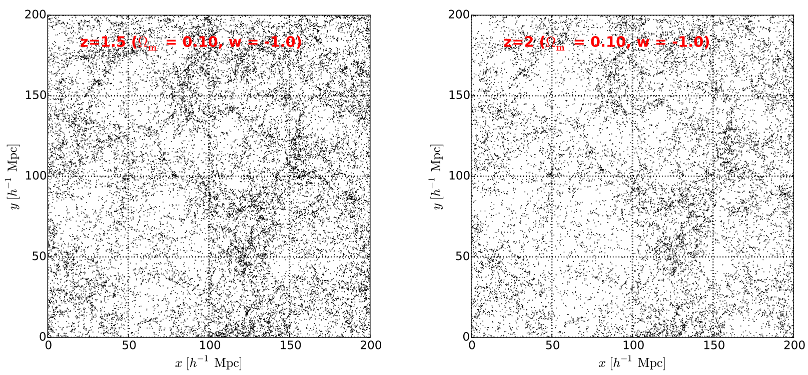

Figure 3. bb

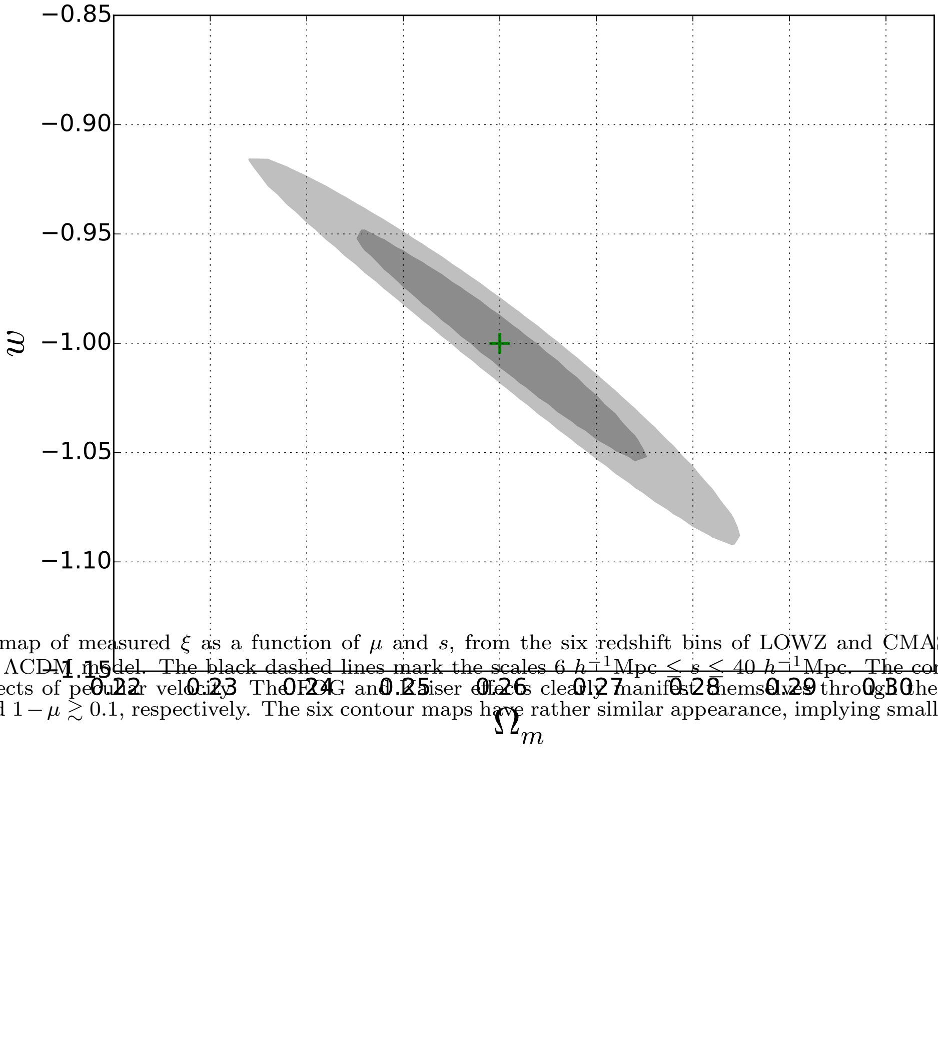

Figure 4. 2D contour map of measured ξ as a function of μ and s, from the six redshift bins of LOWZ and CMASS samples in the cosmology of $\Omega_m = 0.31$ ΛCDM model. The black dashed lines mark the scales 6 h^{-1}Mpc $\leq s \leq$ 40 h^{-1}Mpc. The contour lines are not horizontal due to the effects of peculiar velocity. The FOG and Kaiser effects clearly manifest themselves through the tilting of contour lines where $1-\mu \to 0$ and $1-\mu \gtrsim 0.1$, respectively. The six contour maps have rather similar appearance, implying small redshift evolution of ξ.

where $\hat{\xi}_{\Delta s}(z_i, \mu_j)$ is $\hat{\xi}_{\Delta s}$ measured in the ith redshift bin and jth μ bin, where $1 \leq i \leq 6$ and $1 \leq j \leq n_\mu$. To characterize the shape of the curve well $n_\mu \gtrsim 5$ is required.

4.5. *Correction for systematics*

Other than the AP effect, there are additional effects which may produce redshift-dependent anisotropy and affect the results.

The observational artifacts, such as fiber collisions, redshift failures, and the non-cosmological density fluctuations with stellar density and seeing, are accounted for in the galaxy weights (Reid et al. 2016). Fiber collisions and redshift failures may affect the value of $\hat{\xi}(\mu)$ in the region close to LOS; we abandon the angular region of $1-\mu < 0.01$, to avoid possible systematics (see Appendix **??** for more discussion).

The non-contiguous NGC and SGC are less well cross-calibrated with respect to each other than they are internally calibrated (Schlafly et al. 2010; Schlafly & Finkbeiner 2011; Parejko et al. 2013). We construct the NGC and SGC mock surveys separately to avoid possible systematics. The 2pCF analysis is also carried out for the NGC and SGC independently. The result should be robust as long as each catalogue is well calibrated internally.

The apparent anisotropy introduced by RSD is, although greatly reduced by focusing on the redshift evolution, still the most significant systematic effect.

We estimate the value of $\delta\hat{\xi}_{\Delta s}$ from the systematic effects and subtract their contribution (hereafter $\delta\hat{\xi}_{\Delta s,\rm sys}$) from the total variation. The quantity $\delta\hat{\xi}_{\Delta s,\rm sys}$ is estimated from the HR4 mock galaxies. The mock survey sample imitates the SDSS BOSS sample by mimicking the survey as close as possible and includes past light cone effects. The observational systematics such as the RSD, survey geometry, and shot noise are included in the exactly same way as the observation. The peculiar velocity perturbs the observed redshift through the relation

$$\Delta z = (1+z)\frac{v_{\rm LOS}}{c}, \tag{8}$$

where $v_{\rm LOS}$ is the LOS component of the peculiar velocity of galaxies. The redshift evolution of galaxy peculiar velocities, resulting from growth of structure, causes the anisotropy produced by RSD to have a small redshift evolution; this is the main source of systematic uncertainty in our results.

We take the HR4 mock galaxy samples and compute $r(z)$ of galaxies in the cosmology under which the simulation is based. In this case there is no AP effect. Thus, the measured $\delta\hat{\xi}_{\Delta s}$ are the redshift evolution purely created by systematics effects. They are adopted as the estimation of $\delta\hat{\xi}_{\Delta s,\rm sys}$, and the results are illustrated in Figure 7.

For the 1st to 5th redshift bins, $\delta\hat{\xi}_{\Delta s,\rm sys}(z_i, z_1) \lesssim 0.02$, indicating a small redshift evolution of the RSD effect and properties of galaxies. The only exception is the 6th redshift bin where the values of $\delta\hat{\xi}_{\Delta s,\rm sys}(z_6, z_1)$ are relatively large. The reason for the large values is that the galaxies in that highest redshift bin are significantly more massive than those at lower redshifts, so the measured high redshift $\hat{\xi}_{\Delta s}(\mu)$ has larger (smaller) values at $\mu \to 1$ ($\mu \to 0$) compared with the others (an investigation of the dependence of $\hat{\xi}_{\Delta s}(\mu)$ on galaxy mass is provided in Sec. 4.6).

4.6. *The caveats*

Li et al. (2014, 2015) found the RSD effect exhibits a small redshift dependence of $\hat{\xi}_{\Delta s}(\mu)$, mainly due to the structure growth and the selection effect (different galaxy bias at different redshifts). In this analysis we use the mock galaxy sample from HR4 to correct this systematics. The galaxy assignment scheme of Hong et al. (2016) applied to HR4 is very successful in modeling both the large scale Kaiser effect and the small scale FOG effect in nonlinear regions.

There are two possible caveats in our procedure of the modeling of the RSD effect.

1) The RSD effect is estimated from mock survey samples created in a particular cosmology, i.e., the $\Omega_m = 0.26$ ΛCDM model. If this adopted cosmology is different from the truth, then there could be a systematic bias in the estimation. We believe that this will not seriously affect our cosmological constraints. Li et al. (2014) shows that the redshift dependence of RSD is not sensitive to cosmological parameters. Also, the cosmologies adopted in the HR3 and HR4 simulations are consistent with our best-fit cosmological parameters within 1σ, therefore our inferred cosmological constraints should be fairly accurate. In a future analysis, we will estimate the redshift evolution of the RSD effect from a set of cosmological simulations covering the relevant part of the parameter space. This approach will remove the remaining uncertainty associated with the RSD effect, which is already a minor effect in our analysis.

2) The selection effect, i.e., the evolution of galaxy bias with redshifts, can introduce redshift evolution in the clustering properties of the observed galaxies. In our analysis the amplitude of the 2pCF is normalized and only its angular information, the function $\hat{\xi}_{\Delta s}(\mu)$, is used. This function is rather insensitive to the galaxy bias, which mainly affects the strength of clustering.

As a test, Figure **??** shows $\hat{\xi}_{\Delta s}(\mu)$ measured from a small HR4 galaxy sample with different minimal mass cuts. The mock galaxies are taken from the $z = 0$ snapshot data within the radius $r < 600\ h^{-1}$Mpc. Applying the minimal mass cuts of $1, 2, 4 \times 10^{13} h^{-1} M_\odot$, we created three sets of subsamples with number density of $\bar{n} = 4.56,\ 2.10,\ 0.91 \times 10^{-4} (h^{-1}{\rm Mpc})^{-3}$, which roughly covers the scatter of the number density of BOSS DR12 galaxies at $0.15 < z < 0.7$ [2].

For subsamples with higher mass cuts the $\hat{\xi}_{\Delta s}(\mu)$ has larger (smaller) values at $\mu \to 1$ ($\mu \to 0$). More massive samples result in less tilted $\hat{\xi}_{\Delta s}(\mu)$ in the region of $1-\mu \gtrsim 0.1$ [3]. This explains the relative large value of

[2] The BOSS LOWZ and CMASS galaxies reside in massive haloes with a mean halo mass of $5.2 \times 10^{13} h^{-1} M_\odot$ and $2.6 \times 10^{13} h^{-1} M_\odot$ (Parejko et al. 2013; White 2011; Reid et al. 2016), respectively. For CMASS galaxies, when the redshift changes from $z = 0.43$ to 0.7, the mean stellar mass varies from $10^{11.6} M_\odot$ to $10^{11.9} M_\odot$ (Parihar et al. 2014).

[3] This phenomenon is understandable. The tilt of $\hat{\xi}_{\Delta s}(\mu)$ is related to the RSD effect, and also the overall amplitude of the 2pCF (the denominator of Eq. (6)). The slope should be roughly proportional to $(v/b_g)^2$, where the peculiar velocity term v^2 denotes the effect of RSD, and the galaxy bias term b_g^2 represents the amplitude of the 2pCF. For the more massive sample, b_g is much larger while v is still close to the peculiar velocity of dark matter field, therefore the slope is smaller.

$\hat{\xi}_{\Delta s,\mathrm{sys}}(z_6, z_1)$. In particular, comparing the subsamples with mass cuts $4\times10^{13}h^{-1}M_\odot$ and $1\times10^{13}h^{-1}M_\odot$, we find the red dotted curve is higher (lower) than the blue solid line at $\mu\to1$ ($\mu\to0$), with a difference of $\approx$0.1 (0.05), consistent with the value of $\hat{\xi}_{\Delta s,\mathrm{sys}}(z_6, z_1)$ shown in Figure 7.

In addition, this result also explains the small discrepancy between the $\hat{\xi}_{\Delta s}(\mu)$ measured from the observational data and the HR4 simulations (Figure **??**). The mock galaxies could be systematically more massive than the observed ones. These systematics could be most significant in the 6th redshift bin where mock galaxies are most massive, leading to possible overestimation of $\delta\hat{\xi}_{\Delta s,\mathrm{sys}}$. We discuss the impact of this effect in Sec. 6.1.

Considering the large variation of mass cuts, the change of $\hat{\xi}_{\Delta s}(\mu)$ is not significant, so we conclude that $\hat{\xi}_{\Delta s}(\mu)$ is relatively insensitive to the galaxy bias.

4.7. χ^2 *function*

We define a χ^2 function to quantify the redshift evolution of clustering anisotropy

$$\chi^2 \equiv \sum_{i=2}^{6}\sum_{j_1=1}^{n_\mu}\sum_{j_2=1}^{n_\mu} \mathbf{p}(z_i,\mu_{j_1})(\mathbf{Cov}_i^{-1})_{j_1,j_2}\mathbf{p}(z_i,\mu_{j_2}), \quad (9)$$

where $\mathbf{p}(z_i,\mu_j)$ is the redshift evolution of clustering, $\hat{\xi}_{\Delta s}$, with systematic effects subtracted

$$\mathbf{p}(z_i,\mu_j) \equiv \delta\hat{\xi}_{\Delta s}(z_i,z_1,\mu_j) - \delta\hat{\xi}_{\Delta s,\mathrm{sys}}(z_i,z_1,\mu_j) \quad (10)$$

$\mathbf{Cov}_i$ is the covariance matrix estimated from the 72 sets of PSB mock galaxies identified from HR3 N-body simulation.

4.8. *Cosmological Constraints*

We constrain Ω_m and w through Bayesian analysis (Christensen et al. 2001), which derives the probability distribution function (PDF) of some parameters θ (=(Ω_m, w) in this paper) given observational data $\mathbf{D}$, according to Bayes' theorem:

$$P(\theta|\mathbf{D}) = \frac{P(\theta)P(\mathbf{D}|\theta)}{m(\mathbf{D})}. \quad (11)$$

Here $P(\theta)$, the prior distribution of the parameters, contains all the information about the parameters known from substantive knowledge and expert opinion *before* observing the data. The marginal PDF of $\mathbf{D}$, $m(\mathbf{D}) = \int P(\mathbf{D}|\theta)P(\theta)d\theta$, is a normalization constant independent of θ. All the information about the parameter θ that stems from the experiment is contained in the function $P(\mathbf{D}|\theta)$, the conditional PDF of the observation $\mathbf{D}$ given the value of parameter.

In this analysis we simply assume flat priors for Ω_m and w, and approximate $P(\mathbf{D}|\theta)$ by a likelihood function $\mathcal{L}$ satisfying $-2\ln\mathcal{L} = \chi^2$; the PDF of θ derived from our AP method takes the form

$$P(\theta|\mathbf{D}) \propto \mathcal{L} \propto \exp\left[-\frac{\chi^2}{2}\right]. \quad (12)$$

We use the `COSMOMC` software (Lewis & Bridle 2002) to obtain the Markov Chain Monte Carlo (MCMC) samples of θ following the PDF of $P(\theta|\mathbf{D})$. Constraints on Ω_m and w are derived from these samples.

The 68% and 95% likelihood contours of Ω_m and w obtained from this analysis are shown in Figure **??** (pink areas). Our AP method yields tight constraints on Ω_m and w . The mean values and 68% CL are

$$\Omega_m = 0.314 \pm 0.038, \quad w = -1.09 \pm 0.14. \quad (13)$$

This result is consistent with the Planck ΛCDM cosmology within 1σ (Ade et al. 2015).

5. CONCLUDING REMARKS

* Can be combined with our redshift dependence of AP to full explore the geometric effects in LSS

* *** utilizes angular 2pCF as a function of redshift. Our method is complementary to it: 1) smaller scales; 2) more bins; 3) could be less affected by RSD; ... In case of good modelling of RSD one can rely on their; in case not possible, especially on small scales, one can use ours

* Complementary to all other LSS probes

* Promising future

ACKNOWLEDGMENTS

We thank the Korea Institute for Advanced Study for providing computing resources (KIAS Center for Advanced Computation Linux Cluster System). We would like to thank Yi Zheng for useful discussions. This work was partially supported by the Supercomputing Center/Korea Institute of Science and Technology Information with supercomputing resources including technical support (KSC-2013-G2-003).

APPENDIX

REFERENCES

Ade, P.A.R., Aghanim, N., & Arnaud, M., et al. arXiv:1502.01589
Alam, S., Ata, M., & Bailey, S., et al. 2016, submitted to MNRAS (arXiv:1607.03155)
Alam S., Albareti, F.D.,& Allende Prieto, C., et al., 2015, ApJS, 219, 12
Alcock, C., & Paczynski, B. 1979, Nature, 281, 358
Anderson, L., Aubourg, É., & Bailey, S. et al. 2014, MNRAS, 441, 24
Ballinger, W.E., Peacock, J.A., & Heavens, A.F. 1996, MNRAS, 282, 877
Betoule, M., Kessler, R., & Guy, J., et al. 2014, A&A, 568, 32
Beutler, F., Blake, C., & Colless, M., et al. 2011, MNRAS, 416, 3017
Beutler, F., Saito, S., & Seo, H.-J., et al. 2013, MNRAS, 443, 1065
Beutler, F., Seo, H.-J., & Saito, S., et al. 2016, arXiv:1607.03150
Blake, C., Glazebrook, K., & Davis, T. M., 2011, MNRAS, 418, 1725
Blake, C., James, J.B., & Poole, G.B. 2013, MNRAS, 437, 2488
Bolton, A.S., Schlegel, & D.J., Aubourg E., et al. 2012, AJ, 144, 144
Boylan-Kolchin, M., Ma, C.-P., & Quataert, E. 2008, MNRAS, 383, 93
Christensen, N., Meyer, R., Knox, L., & Luey, B. 2001, Class. Quant. Grav., 18, 2677
Chuang, C.-H., & Wang, Y. 2012, MNRAS, 426, 226
Dawson, K.S., Kneib, J.P., & Percival, W.J., et al. 2015, accepted AJ
Dawson, K.S., Schlegel, D.J., & Ahn, C.P., et al. 2012, AJ, 145, 10
Efstathiou, G. 2014, MNRAS, 440, 1138

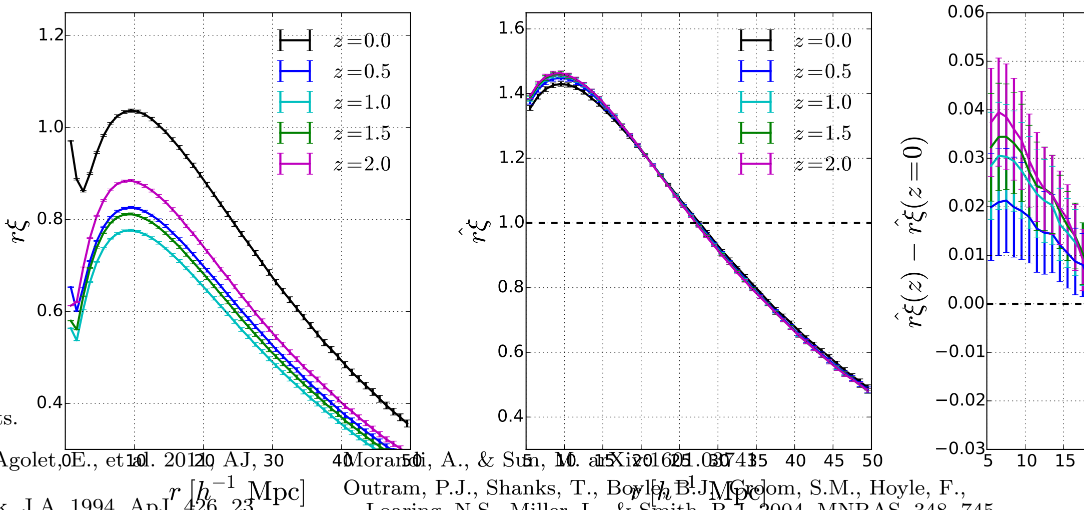

Figure 5. 2pCF at different redshfits.

Eisenstein, D.J., Weinberg, D.H., & Agol, E., et al. 2011, AJ, 142, 72
Feldman, H.A., Kaiser, N., & Peacock, J.A. 1994, ApJ, 426, 23
Fukugita, M., Ichikawa, T., & Gunn, J.E., et al. 1996, AJ, 111, 1748
Gunn, J.E., Carr, M., & Rockosi, C. et al. 1998, AJ, 116, 3040
Gunn, J.E., Siegmund, W.A., & Mannery, E.J., et al. 2006, AJ, 131, 2332
Guzzo, L., Pierleoni, M., & Meneux, B., et al. 2008, Nature, 451, 541
Hartlap J., Simon P. & Schneider P. [astro-ph/0608064].
Hong, S.E., Park, C.,& Kim, J. 2016, ApJ, 823, 103
Jackson, J., 1972, MNRAS, 156, 1
Jennings, E., Baugh, C.M., & Pascoli, S. 2011, MNRAS, 420, 1079
Jiang, C.Y., Jing, Y. P., & Faltenbacher, A., et al. 2008, ApJ, 675, 1095
Kaiser, N. 1987, MNRAS, 227, 1
Kim, J., & Park, C. 2006, ApJ, 639, 600
Kim, J., Park, C., Gott, J.R., III, & Dubinski, J. 2009, ApJ, 701, 1547
Kim, J., Park, C., L'Huillier, B., & Hong, S. E. 2015, JKAS, 48, 213
Kim, J., Park, C., Rossi, G., Lee, S.M., & Gott, J.R. 2011, JKAS, 44, 217
Kitaura, F.S., Rodríguez-Torres, S., Chuang, C.-H., et al. arXiv:1509.06400
Komatsu, E., Smith, K. M., & Dunkley, J., et al. 2011, ApJS, 192, 18
Lacey, C., & Cole, S. 1993, MNRAS, 262, 627
Landy, S.D., & Szalay, A.S. 1993, ApJ, 412, 64
Laureijs, R., Amiaux, J., & Arduini, S., et al. 2011, arXiv:1110.3193
Lavaux, G., & Wandelt, B.D. 2012, ApJ, 754, 109
Lewis, A., & Bridle, S. 2002, Phys. Rev. D, 66, 103511
L'Huillier, B., Park, C., & Kim, J. 2014, New Astronomy, 30, 79
Li, M., Li, X.-D., Wang, S., & Wang, Y. 2011, Commun. Theor. Phys., 56, 525
Li, X.-D., Park, C., Forero-Romero, J., & Kim, J. 2014, ApJ, 796, 137
Li, X.-D., Park, C., Sabiu, C.G., & Kim, J. 2015, MNRAS, 450, 807
Li, X.-D., Park, C., Sabiu, C.G., & Kim, J. 2016, submitted to ApJ
Linder, E.V., Minji, O., Okumura, T., Sabiu, C.G., & Song, Y.-S. 2014, Phys. Rev. D, 89, 063525
López-Corredoira, M. 2014, ApJ, 781, 96
Marinoni, C., & Buzzi, A. 2010, Nature, 468, 539
Matsubara T., & Suto, Y. 1996, ApJ, 470, L1
McCavana, T., Micic, M., Lewis, G. F., et al. 2012, MNRAS, 424, 361
Morandi, A., & Sun, M. arXiv:1601.03741
Outram, P.J., Shanks, T., Boyle, B.J., Croom, S.M., Hoyle, F., Loaring, N.S., Miller, L., & Smith, R.J. 2004, MNRAS, 348, 745
Parejko J.K., et al., 2013, MNRAS, 429, 98
Parihar, P., Vogeley, M.S., & Gott, J.R., et al. 2014, ApJ, 796, 86
Park, C., Kim, J., & Gott, J.R. 2005, ApJ, 633, 1
Park, C., & Kim, Y.-R. 2010, ApJL, 715, L185
Park, C., Choi, Y.-Y., Kim, J., Gott, J.R., Kim, S.S., & Kim, K.-S. 2012, ApJ, 759, 7
Park, C., Song, H., Einasto, M., Lietzen, H., & Heinamaki, P. 2015, JKAS, 48, 75
Peebles, P.J.E., & Ratra, B. 2003, Reviews of Modern Physics, 75, 559
Percival, W.J., Ross, A.J., & Sánchez, A.G., et al. 2014, MNRAS, 439, 2531
Perlmutter, S., Aldering, G., & Goldhaber, G., et al. 1999, ApJ, 517, 565
Press, W.H., & Schechter, P.L. 1974, ApJ, 187, 425
Reid, B., Samushia, L., & White, M., et al. 2012, MNRAS, 426, 2719
Reid, B., Ho, S., & Padmanabhan, N., et al. 2016, MNRAS, 455, 1553
Riess, A.G., Filippenko, A.V., & Challis, P., et al. 1998, AJ, 116, 1009
Riess, A.G., Macri, L., & Casertano, S., et al. 2011, ApJ, 730, 119
Ross, A.J., Percival, W.J., & Sánchez, A.G. et al. 2012, MNRAS, 424, 564
Ross, A.J., Samushia, L., & Howlett, C., et al. 2015, MNRAS, 449, 835
Ryden, B.S. 1995, ApJ, 452, 25
Sanchez, A. G., Scoccimarro, R., & Crocce, M., et al. arXiv:1607.03147
Schlafly E.F., Finkbeiner D.P., Schlegel D.J., et al. 2010, ApJ, 725, 1175
Schlafly E.F., & Finkbeiner D.P. 2011, ApJ, 737, 103
Schlegel, D., Abdalla, F., & Abraham, T., et al. 2011, arXiv:1106.1706
Smee, S.A., Gunn, J.E., & Uomoto, A., et al. 2013, AJ, 146, 32
Song, Y.S., Sabiu, C.G., Okumura, T., Oh, M., & Linder, E.V. 2014, JCAP, 12, 005
Speare, R., Gott, J.R., Kim, J., & Park, C. 2015, ApJ, 799, 176
Viana, P.T.P., & Liddle, A.R. 1996, MNRAS, 281, 323
Villalobos, Á., De Lucia, G., Weinmann, S.M., Borgani, S., & Murante, G. 2013, MNRAS, 433, L49
Weinberg, S. 1989, Reviews of Modern Physics, 61, 1
White M., et al. 2011, ApJ, 728, 126
York, D.G., Adelman, J., & Anderson, J.E., et al. 2000, AJ, 120, 1579
Zehavi, I., Zheng, Z., & Weinberg, D.H., et al. 2011, ApJ, 736, 59

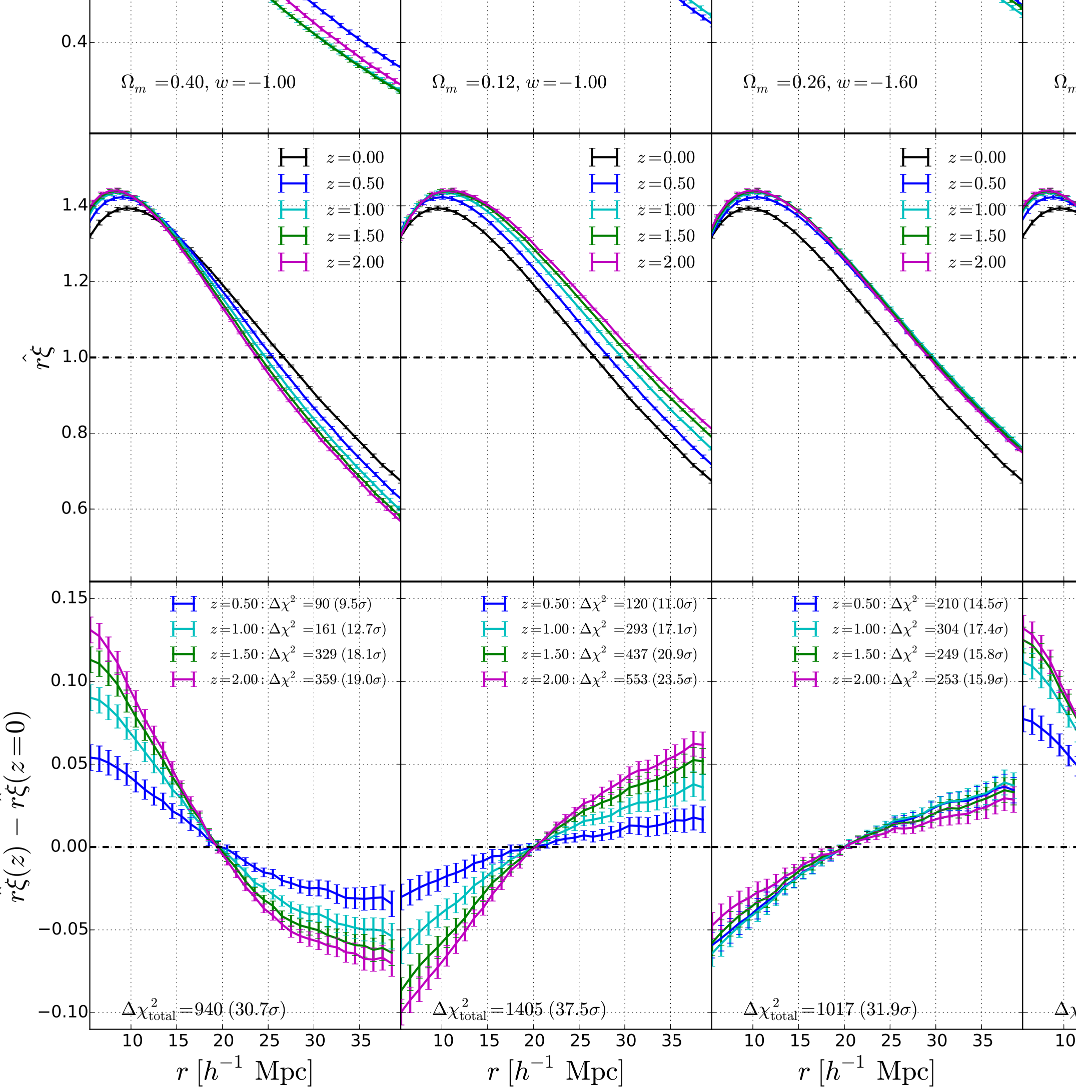

Figure 6. 2pCF in cosmologies.

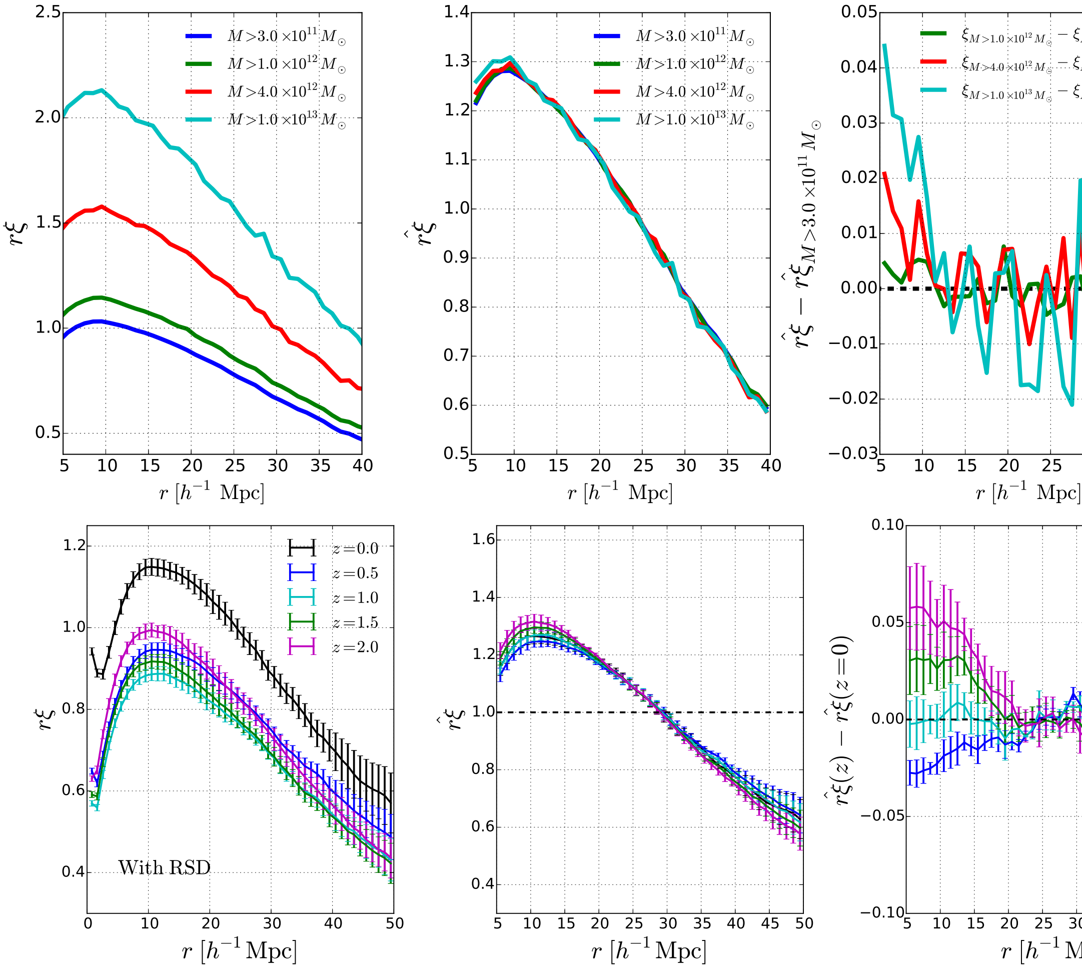

Figure 7. Systematic effects.

Figure 8. Likelihood contours (68.3%, 95.4%) in the $\Omega_m - w$ plane from our method.